2004

Variability in springtime thaw in the terrestrial high latitudes: Monitoring a major control on the biospheric assimilation of atmospheric CO2 with spaceborne microwave remote sensing

Kyle C. McDonald
City College of New York

John S. Kimball
University of Montana - Missoula

Eni G. Njoku

Reiner Zimmermann

Maosheng Zhao

Recommended Citation

McDonald, K., J. Kimball, E. Njoku, R. Zimmermann, and M. Zhao, 2004: Variability in Springtime Thaw in the Terrestrial High Latitudes: Monitoring a Major Control on the Biospheric Assimilation of Atmospheric CO2 with Spaceborne Microwave Remote Sensing. Earth Interact., 8, 1–23, doi: 10.1175/1087-3562(2004)8<1:VISTIT>2.0.CO;2

Variability in Springtime Thaw in the Terrestrial High Latitudes: Monitoring a Major Control on the Biospheric Assimilation of Atmospheric CO_2 with Spaceborne Microwave Remote Sensing

Kyle C. McDonald*
Jet Propulsion Laboratory, California Institute of Technology, Pasadena, California

John S. Kimball
Flathead Lake Biological Station, Division of Biological Sciences, University of Montana, Polson, and Numerical Terradynamic Simulation Group, University of Montana, Missoula, Montana

Eni Njoku
Jet Propulsion Laboratory, California Institute of Technology, Pasadena, California

Reiner Zimmermann
Max-Planck-Institute for Biogeochemistry, Jena, Germany

Maosheng Zhao
Numerical Terradynamic Simulation Group, University of Montana, Missoula, Montana

Received 27 February 2004; accepted 19 April 2004

* Corresponding author address: Kyle C. McDonald, Jet Propulsion Laboratory, California Institute of Technology, Mail Stop 300-233, 4800 Oak Grove Drive, Pasadena, CA 91101.
E-mail address: kyle.mcdonald@jpl.nasa.gov

ABSTRACT: Evidence is presented from the satellite microwave remote sensing record that the timing of seasonal thawing and subsequent initiation of the growing season in early spring has advanced by approximately 8 days from 1988 to 2001 for the pan-Arctic basin and Alaska. These trends are highly variable across the region, with North America experiencing a larger advance relative to Eurasia and the entire region. Interannual variability in the timing of spring thaw as detected from the remote sensing record corresponded directly to seasonal anomalies in mean atmospheric CO_2 concentrations for the region, including the timing of the seasonal draw down of atmospheric CO_2 from terrestrial net primary productivity (NPP) in spring, and seasonal maximum and minimum CO_2 concentrations. The timing of the seasonal thaw for a given year was also found to be a significant ($P < 0.01$) predictor of the seasonal amplitude of atmospheric CO_2 for the following year. These results imply that the timing of seasonal thawing in spring has a major impact on terrestrial NPP and net carbon exchange at high latitudes. The initiation of the growing season has also been occurring earlier, on average, over the time period addressed in this study and may be a major mechanism driving observed atmospheric CO_2 seasonal cycle advances, vegetation greening, and enhanced productivity for the northern high latitudes.

KEYWORDS: Remote sensing, Net primary production, Freeze thaw

1. Introduction

Each spring, approximately 50 million km^2 of Earth's terrestrial Northern Hemisphere undergoes a seasonal transition from predominantly frozen to nonfrozen (i.e., thawed) conditions (Robinson et al. 1993). These relatively abrupt seasonal transitions represent the closest analog to a biospheric and hydrologic on/off switch existing in nature, profoundly affecting surface meteorological conditions, ecological trace gas dynamics, energy exchange, and hydrologic activity. Boreal and Arctic regions form a complex land-cover mosaic where vegetation structure, condition, and distribution are strongly regulated by environmental factors such as soil moisture and nutrient availability, permafrost, growing season length, and disturbance. In seasonally frozen environments, the growing season is determined primarily by the length of the nonfrozen period. Variations in both the timing of spring thaw and the resulting growing season length have been found to have a major impact on terrestrial carbon exchange and atmospheric CO_2 source/sink strength in boreal regions (Frolking et al. 1996; Randerson et al. 1999). The timing of spring thaw, in particular, can influence boreal carbon uptake dramatically through temperature and moisture controls to net photosynthesis and respiration processes (Jarvis and Linder 2000; Tanja et al. 2003). With boreal evergreen forests accumulating approximately 1% of annual net primary productivity (NPP) each day immediately following seasonal thawing, variability in the timing of spring thaw can trigger total interannual variability in carbon uptake on the order of 30% (Frolking et al. 1996; Kimball et al. 2004a). Temporal variations in the onset of frozen conditions in the fall are also significant but generally have less impact on annual productivity due to the increased

importance of other controls on vegetation photosynthetic activity such as photoperiod length (Kimball et al. 2004a).

Frolking et al. (Frolking et al. 1996) evaluated the range of interannual variability of boreal forest growing season length and associated impacts on carbon and water fluxes and found that earlier spring thaws led to significant increases in simulated net carbon uptake. Soil temperature simulations from 1976 to 1996 for boreal forest stands show 6–7-week ranges in the timing of snowmelt and soil thaw at 3 cm, equivalent to a year-to-year change in growing season length of 30%. At the Boreal Ecosystem–Atmosphere Study (BOREAS) southern study area old aspen site in Saskatchewan, Canada, the transition of the ecosystem from a carbon source ($\sim +25$ kg C ha^{-1} day^{-1}) to its maximum rate of carbon uptake (–75 kg C ha^{-1} day^{-1}) occurs over a 10-day period in the spring. Subsequent longer-term studies at this site have shown that interannual variations in spring thaw timing, in particular, have a major impact on annual carbon sequestration, primarily through controls on the timing of spring leaf emergence and associated net photosynthesis (Black et al. 2000). Multiyear tower eddy flux measurements of CO_2 exchange over mature boreal black spruce stands indicate that the seasonal switch from a net source to a sink for atmospheric carbon is coincident with snowmelt and associated thawing of the upper soil horizons in the spring (Goulden et al. 1998; Jarvis and Linder 2000). Similarly, regional analyses of boreal annual NPP show a sensitivity to spring thaw timing on the order of 1% day^{-1} immediately following initiation of the growing season (Kimball et al. 2004a). Recent changes observed in the seasonal cycle of atmospheric CO_2 at high northern latitudes have also been attributed to earlier ecosystem carbon uptake and increased NPP associated with warmer springtime air temperatures (Keeling et al. 1996; Randerson et al. 1999; Keyser et al. 2000). A logical step for improved assessment and monitoring of seasonal and year-to-year changes in the net carbon flux for boreal regions would be to determine the timing and variation of freeze–thaw transition periods for improved regional characterization of growing season length and associated terrestrial carbon cycle dynamics.

Atmospheric tracer studies indicate that the terrestrial Northern Hemisphere between 30° and 60° latitude is a significant sink of atmospheric CO_2, though the exact nature of this sink is currently unknown (Tans et al. 1990; Ciais et al. 1995; Keeling et al. 1996; Fan et al. 1998). Recent evidence also indicates that the magnitude and stability of this sink may be changing. Observed increases in the seasonal amplitude of atmospheric CO_2 for the high northern latitudes have been attributed to increased growing season length inferred from observed phase advances in the atmospheric CO_2 concentration record (Keeling et al. 1996; Randerson et al. 1999), tree growth ring analyses (Jacoby et al. 1996), analyses of long-term surface weather records (Keyser et al. 2000), and global vegetation indices and terrestrial NPP derived from the National Oceanic and Atmospheric Administration (NOAA) Advanced Very High Resolution Radiometer (AVHRR) satellite record (Myneni et al. 1997; Nemani et al. 2003). A recent summary of atmospheric general circulation model (GCM) projections indicates an average global warming of the lower troposphere of 1°–3.5°C during the next century, with a maximum warming in high northern latitudes in winter (Houghton et al. 1996). Biospheric responses to these changes are likely to be widespread, with significant

feedbacks to regional- and global-scale weather patterns and carbon cycle dynamics (Pielke and Vidale 1995; Betts et al. 1998; Clark et al. 1999; Watson et al. 1998).

Microwave remote sensing techniques have the capability to monitor large-scale changes in the relative abundance and phase (frozen or thawed) of water at the landscape surface. Satellite microwave remote sensing, unlike optical/near-infrared systems, is directly sensitive to the freeze–thaw state of the land surface, including vegetation, snow, and surface soil, and provides an effective measure of growing season initiation for boreal and subalpine evergreen forests (Kimball et al. 2004a; Kimball et al. 2004b; Running et al. 1999). Satellite remote sensing in visible and near-infrared wavelengths is sensitive to changes in photosynthetic biomass and provides a means for regional mapping and monitoring of seasonal phenology (i.e., bud burst, canopy growth, and senescence) and growing season length for deciduous vegetation (Zhou et al. 2001). Boreal regions, however, are composed predominantly of evergreen coniferous forests that do not exhibit large seasonal variations in photosynthetic biomass. The growing season for evergreen vegetation is limited primarily by the seasonal nonfrozen period, which can be 1–2 months longer than the growing season for deciduous vegetation (Black et al. 2000). Air temperature measurements from regional surface weather station networks can provide a relative measure of growing season length for evergreen vegetation, but regional application of these data is limited by sparse station networks and inconsistent monitoring at high latitudes (Karl 1995).

Coarse-resolution (~25 km) spaceborne scatterometers such as the National Aeronautics and Space Administration (NASA) Scatterometer (NSCAT) and the SeaWinds and Earth Remote Sensing (ERS) scatterometers have demonstrated utility for monitoring and quanitfying freeze–thaw transitions at regional scales with high temporal (daily) precision in northern latitudes (Running et al. 1999; Frolking et al. 1999; Kimball et al. 2001; Kimball et al. 2004a; Kimball et al. 2004b; Wismann 2000). These methods have proven useful for regional assessment of freeze–thaw state and associated hydrological and ecological parameters across Alaska, Canada, and the pan-boreal high-latitude regions (Frolking et al. 1999; Kimball et al. 2004b; Rawlins et al. 2005). A primary objective of NASA's Hydrosphere States (HYDROS) Earth System Science Pathfinder mission is to provide exploratory measurements that constitute global-scale measurement of Earth's land surface freeze–thaw conditions, utilizing L-band radar at higher (3 km) spatial resolution (Entekhabi et al. 2004, manuscript submitted to *IEEE Trans. Geosci. Remote Sens.*, hereafter ENT).

Surface brightness temperature measurements acquired by spaceborne passive microwave radiometry offer the potential for similar investigation of variability in terrestrial freeze–thaw state and associated linkages to biophysical processes for the high latitudes over a much longer historic time series than spaceborne scatterometer data records. Brightness temperature measurements obtained from the Special Sensor Microwave Imager (SSM/I) have been applied in terrestrial cryosphere studies including snow cover extent mapping and frozen soil analyses (e.g., Armstrong and Brodzik 1995; Zhang and Armstrong 2001). In this paper, we utilize SSM/I brightness temperature measurements to examine variability in the timing of springtime thaw across the pan-boreal high latitudes for the time

period 1988–2001. We apply these data to monitor annual variability in springtime thaw, examining the multiyear time series afforded by the retrospective dataset, and compare these results to surface biophysical measurements and seasonal atmospheric CO_2 concentration records from Arctic and subArctic monitoring stations.

2. Methods

The SSM/I is a multifrequency, linearly polarized passive microwave radiometer operating with a constant incidence angle of 53.1° and has flown on the Defense Meteorological Satellite Program (DMSP) platform series. Coverage is global and begins in August 1987. We utilize the 19-GHz horizontally polarized channel, which has a 70 km × 45 km footprint resolution. Data for this study were acquired from the National Snow and Ice Data Center as global daily gridded brightness temperatures derived from orbital (swath) data (Armstrong et al. 1994). Orbital data for each 24-h period are mapped to a 25 km × 25 km resolution Equal-Area Scalable Earth Grid (EASE-Grid) format. The data gridding scheme maximizes the radiometric integrity of the original brightness temperature values, maintains high spatial and temporal precision, and involves no averaging of original swath data. To facilitate large-scale analysis, we define our study domain to be the pan-Arctic terrestrial drainage basin and Alaska (Figure 1). This region extends as far south as 45°N in southern Canada and southern Siberia. The land surface within this region is comprised of 39 926 EASE-Grid cells. Daily SSM/I data, spanning winter 1988 through autumn 2001, were assembled onto a 25-km grid covering the study domain. The daily composite data allow examination of annual thaw cycles from 1988 to 2001.

A material's radiometric brightness temperature T_B is characterized by its emissivity e as $T_B = e \times T$, where T is its physical temperature (K). Emissivity is a unitless variable ranging from 0 for a perfectly nonemitting material to 1 for a perfect emitter (blackbody; Ulaby et al. 1986). Emissivity is a function of the material's dielectric constant and is directly sensitive to the phase (solid/liquid) of water within the media. As water changes from a solid to a liquid phase, its dielectric constant increases dramatically and significant increases in e and T_B result. Defining freeze–thaw as the predominant state (solid or liquid) of water within the landscape, we utilize the temporal change in T_B associated with the primary landscape springtime thaw event to monitor the timing of thaw across the study domain.

Previous studies have employed thresholding schemes based on time series signal processing to examine springtime thaw transitions with high temporal repeat microwave remote sensing data (Frolking et al. 1999; Kimball et al. 2001; Kimball et al. 2004a; Kimball et al. 2004b). These algorithms characterize landscape thaw transition sequences utilizing the response of time series radar backscatter resulting from large changes in the bulk landscape dielectric constant occurring as the landscape thaws. As T_B responds similarly to the landscape dielectric constant, these approaches are also suitable for analysis of time series brightness temperature.

We employ a step edge detection scheme to identify the predominant springtime

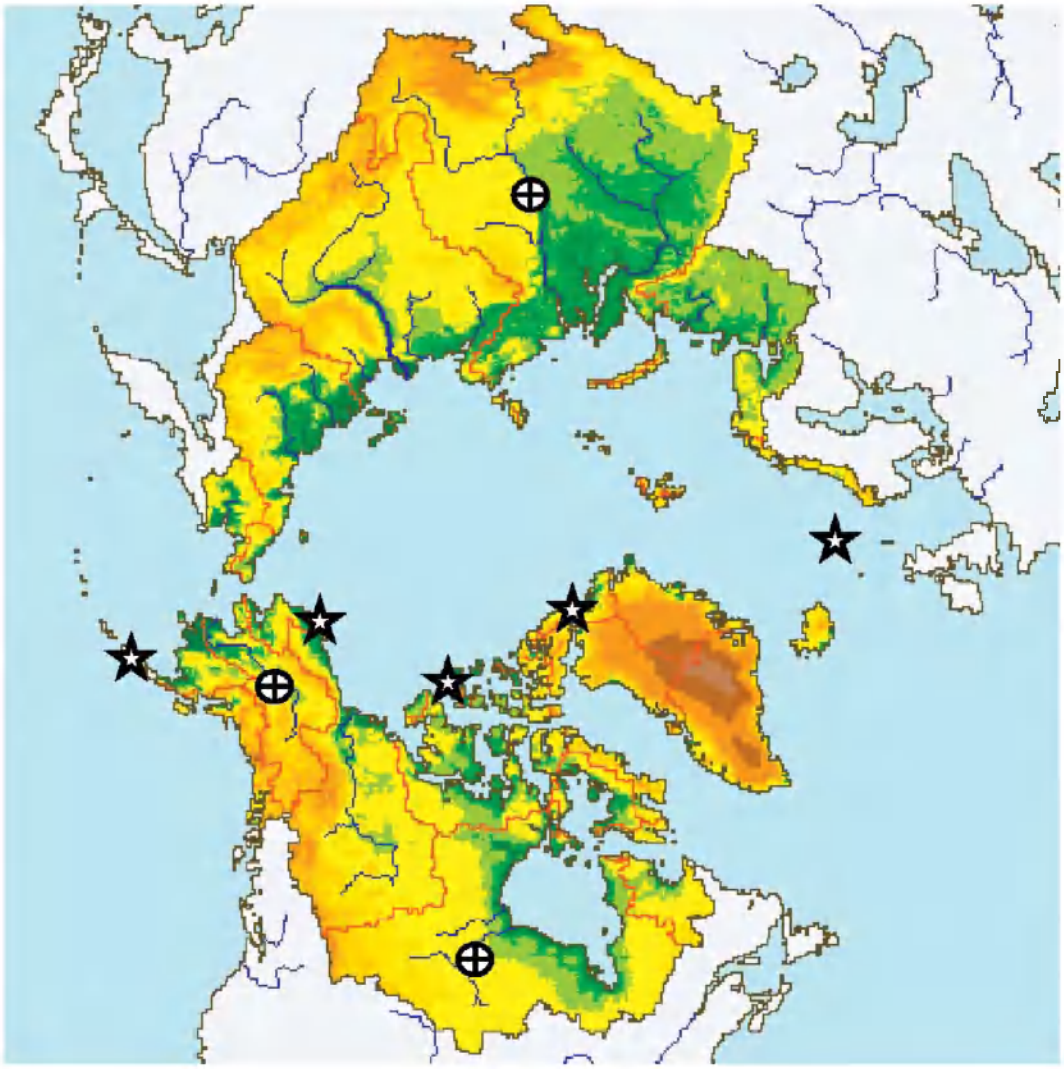

Figure 1. The domain of our study encompasses the terrestrial pan-Arctic drainage basin and Alaska. This map shows the locations of the three biophysical monitoring stations we used for point-scale comparison (indicated by circled crosses) and the five NOAA/CMDL monitoring stations we used for comparison with high-latitude CO_2 patterns (indicated by stars). The terrestrial pan-Arctic drainage is defined as all land areas draining into the Arctic Ocean, Hudson Bay, and the Bering Sea. The study domain encompasses 39 926 EASE-Grid cells, each a 25 km × 25 km equal area.

thaw transition event on an annual basis. In boreal regions this event has been found to be generally coincident with the arrival of maximum surface wetness in spring associated with rising air temperatures, seasonal snowmelt, soil active layer thawing, and growing season onset (Kimball et al. 2004a). The technique is based on the application of an optimal edge detector for determining edge transitions in

noisy signals (Canny 1986). The time of the primary springtime thaw event is determined from the convolution applied to T_B:

$$\mathrm{CNV}(t) = \int_{-\infty}^{\infty} f'(x) T_B(t - x) dx, \tag{1}$$

where $f'(x)$ is the first derivative of a normal (Gaussian) distribution. The occurrence of the primary springtime thaw event is then given by the time t_p, when CNV(t) is a maximum. As the winter–spring transition progresses, the landscape may thaw and refreeze repeatedly. This technique accounts for the occurrence of weak edges, or less pronounced thaw events, as well as strong edges, and is less likely to classify minor thaw occurrences as the primary thaw event. This approach has been previously employed to examine thaw trends in the North American segment of our study domain (McGuire et al. 2004). For this investigation we apply a similar approach to map the spring thaw event on an annual basis for each 25-km grid cell within the entire pan-Arctic basin and Alaska study region.

The thaw classification algorithm was applied to each annual time series of SSM/I brightness temperature from 1988 through 2001, producing yearly maps of the primary spring thaw event across the pan-Arctic basin and Alaska. A linear trend analysis was applied on a grid-cell-by-grid-cell basis to quantify the statistical significance of temporal trends in spring thaw timing over the 14-yr period. Areas of permanent ice and snow, bare ground, and sparse vegetation cover were identified using a 1-km resolution, global land-cover classification (Friedl et al. 2002) and were masked from further analysis to isolate the relationships between seasonal thawing, vegetation growing season dynamics, and associated effects of net photosynthesis on seasonal atmospheric CO_2 patterns. Mean primary thaw dates were determined for each of the 14 yr for the entire pan-boreal study domain, as well as for North American and Eurasian portions of the study region.

Brightness temperature and thaw classification algorithm performance were compared with surface station temperature measurements at three sites in the study domain (Figure 1) where biophysical data were collected: 1) Zotino, Siberia, a pine forest site in west-central Siberia swampland; 2) Bonanza Creek Experimental Forest (BNZ), Alaska, a National Science Foundation (NSF) Long-Term Ecological Research site in interior Alaska; and 3) the BOREAS Northern Old Black Spruce (NOBS) study site in northern Manitoba, Canada. The Zotino flux tower site is located in central Siberia at 60.75°N, 89.38°E on the west side of the Yenisei River, in a Scots pine (*Pinus sylvestris* ssp. *sibirica*) forest within the western Siberian lowlands. The station is located in a 203-yr-old stand within a chronosequence from early succession to senescent stands (Wirth et al. 1999; Zimmermann et al. 2000) and is part of the Terrestrial Carbon Observation System Siberia project (http://www.bgc-jena.mpg.de). The Bonanza Creek station is at 64.70°N, 148.23°W along the Tanana River flood plain in Alaska's central interior, where a dry continental climate dominates. The station monitors conditions in an alluvial spruce-hardwood mosaic forest dominated by black spruce (*Picea mariana*), white spruce (*Picea glauca*), balsam poplar (*Populus balsamifera*), and alder (*Alnus* spec.). The station includes sets of thermistors implanted in the tree boles and at various depths in the soil. The NOBS site is situated at 5.90°N,

198.50°W, in a boreal conifer forest dominated by black spruce (*Picea mariana*), and is part of the AmeriFlux site network (Baldocchi et al. 1996). Data from both the BNZ and NOBS stations have been utilized in previous studies to assess seasonal freeze–thaw transitions in spaceborne scatterometer data and associated links to growing season productivity (Frolking et al. 1999; Kimball et al. 2004b).

We compared SSM/I-derived measurements of pan-Arctic spring thaw timing to seasonal atmospheric CO_2 concentration records from NOAA/Climate Monitoring and Diagnostics Laboratory (CMDL) Arctic and sub-Arctic monitoring stations (Figure 1) to assess the role of spring thaw timing in regulating high-latitude CO_2 seasonal patterns. Mean monthly CO_2 records were extracted for the Point Barrow (71°N), Ocean Station (66°N), Cold Bay (55°N), Alert (82°N), and Mould Bay (76°N) stations (Table 1; Conway et al. 1994). A plot of mean monthly atmospheric CO_2 concentrations and standard error bars for these five high-latitude monitoring stations is presented in Figure 2. Previous studies have shown that the seasonal atmospheric CO_2 cycle at high northern latitudes is dominated largely by northern terrestrial ecosystems, with minimal impacts from ocean exchange, fossil fuel emissions, and tropical biomass burning (Randerson et al. 1997; Heimann et al. 1998; Erickson et al. 1996). The average of the five stations' mean monthly records was normalized as the difference between monthly and mean annual CO_2 concentrations for each year. We extracted a set of variables from each station record describing the shape of the yearly seasonal CO_2 pattern (Figure 3) including minimum (*A*) and maximum (*B*) seasonal CO_2 concentrations; timing of annual downward (*C*) and upward (*D*) 0-ppm crossings and the period between these and respective crossing dates (*E*); differences between the annual trough and proceeding (*F*) and following (*G*) crests of each seasonal CO_2 cycle and their respective ratio (*H*). Variables *A* and *B* provide a relative measure of maximum seasonal respiration and net carbon uptake rates, while *C*, *D*, and *E* are respective surrogates for the timing of growing season initiation, termination, and length (Keeling et al. 1996; Randerson et al. 1997); variables *F*, *G*, and *H* provide relative measures of semiannual net photosynthesis, net respiration, and their ratio (Hall et al. 1975; Hanqin et al. 2000). Each seasonal shape parameter was derived from individual station records, averaged on a yearly basis across all stations, and compared with pan-Arctic averages of SSM/I spring thaw results. Annual anomalies of SSM/I and CMDL station results were calculated relative to long-term means or linear least squares regression results where significant secular trends were observed. Significance was assessed based on a 90% probability level.

Table 1. NOAA/CMDL mean monthly station records (Conway et al. 1994) used to evaluate northern high-latitude atmospheric CO_2 seasonal patterns and SSM/I primary thaw date anomalies.

Station name	Station abbreviation	Latitude (°N)	Longitude (°W)	Available record
Point Barrow	BRW	71.32	156.10	1988–2001
Ocean Station	STM	66.00	-2.00	1988–2001
Cold Bay	CBA	55.20	162.72	1988–96, 2001
Alert	ALT	82.45	62.52	1988–2001
Mould Bay	MBC	76.23	119.33	1988–96

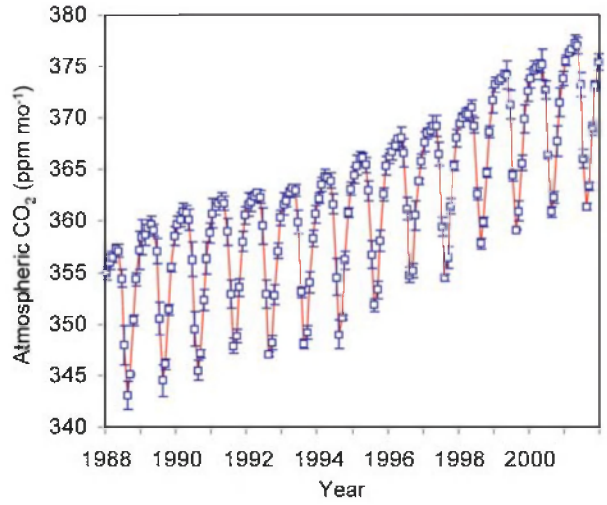

Figure 2. The long-term (1988–2001) record of pan-Arctic mean monthly atmospheric CO_2 concentrations (ppm). The atmospheric CO_2 concentrations shown are the average of monthly mean values recorded at five NOAA/CMDL Arctic and sub-Arctic monitoring stations. The error bars denote standard deviations of mean monthly values across all sites. These records exhibit an average seasonal range of 4% (15 ppm) and a 5.4% (19 ppm) secular increase in mean annual CO_2 over the 14-yr study period.

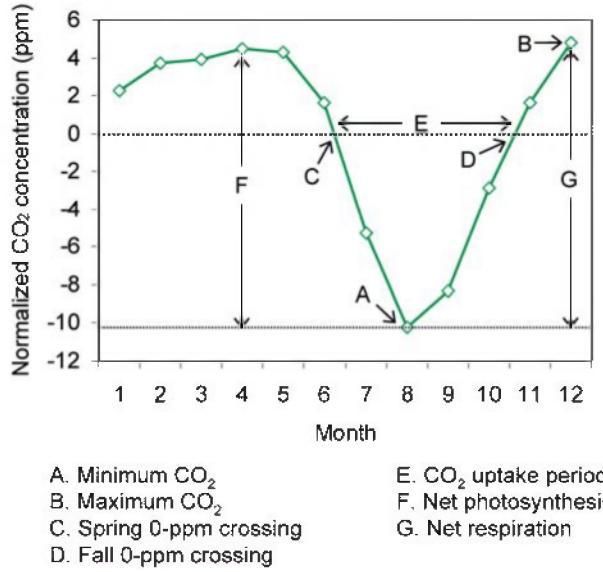

Figure 3. Example of the normalized (monthly – annual mean) NOAA/CMDL atmospheric CO_2 seasonal record identifying the shape parameters used to assess the linkages between SSM/I-derived primary thaw and atmospheric CO_2 seasonal cycle anomalies.

Relationships between annual anomalies in spring thaw timing and seasonal CO_2 patterns were then evaluated accordingly.

3. Results and discussion

The slopes of the least squares regression relationships, mapped on a grid-cell-by-grid-cell basis, provided a measure of the rate of change in annual thaw day for each grid cell across the study domain and are shown in Figure 4. Areas of permanent ice and snow, bare land, and sparse vegetation cover are shown masked in gray. Approximately 75% of the study region showed advancing trends in the timing of seasonal thaw, while 25% of the region showed neutral or delayed trends in spring thaw. Figure 5 provides a map of the statistical significance of these

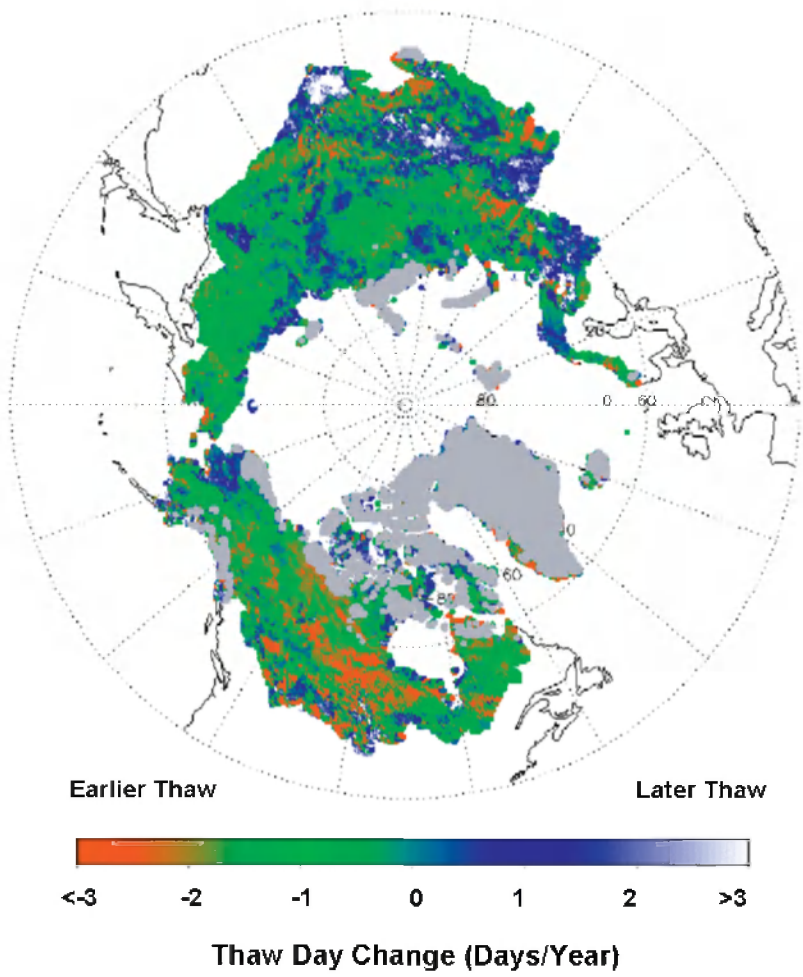

Figure 4. Map of the multiyear trend in thaw day across the pan-boreal study domain excluding permanent ice and snow, barren, and sparsely vegetated areas (indicated in gray). Areas experiencing pronounced advance toward earlier thaw are indicated in red, while blue and white regions tend toward later thaw.

trends. Spatial analysis of these relationships shows that the thaw trends are significant at the 90% probability level over approximately 31% of the unmasked study region, with significance being greater than 95% over approximately 20% of the region. Although comprising only 38% of the masked study region, the majority (53%) of the advances significant at the 90% probability level occur across Canada and Alaska, while significant trends are more dispersed across Eurasia, with both advancing and delayed trends in spring thaw. Linear regression

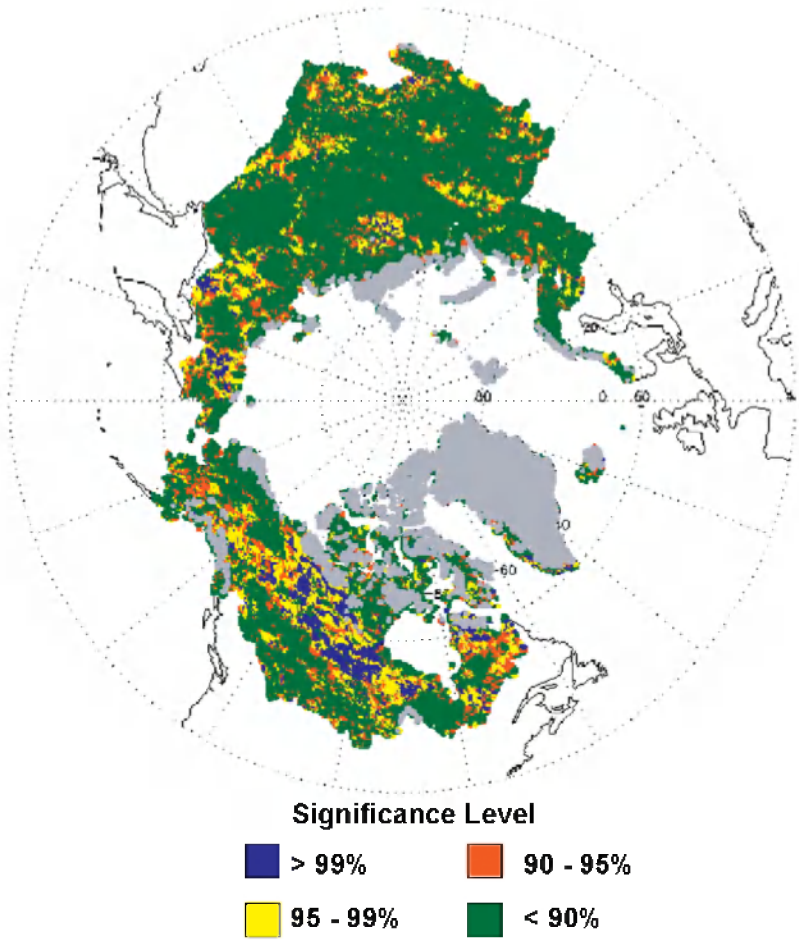

Figure 5. Map of statistical significance of the thaw trends across the study domain excluding permanent ice and snow, barren, and sparsely vegetated areas (indicated in gray). Levels of significance of the least squares linear regression relationships between SSM/I thaw date and year (independent variable) for the 1988–2001 time series were determined for each 25-km grid cell. Excluding the masked areas (in gray), 6.2% of the region showed significance levels above 99% (in blue); 13.3% showed levels between 95% and 99% (yellow), and 11.1% showed levels between 90% and 95% (red). Regions shown in dark green make up 69.4% of the study domain and are those areas for which trends had less than 90% significance.

analyses of regionally averaged data elucidate a general trend toward earlier springtime thaw (Figure 6). These results indicate that the average primary spring thaw event for the pan-Arctic study region advanced by 0.60 days yr^{-1}, or nearly 8 days over the 14-yr study period ($R^2 = 0.356$; $P = 0.024$). The timing of spring thaw for the North American portion of the study region advanced at a faster rate of 0.94 days yr^{-1} ($R^2 = 0.487$; $P = 0.005$), for a total advance of approximately 13 days over the 14-yr study period. The average spring thaw advance for Eurasia was relatively small compared to North America and the larger study region; the spring thaw advance for Eurasia occurred at a statistically insignificant ($R^2 = 0.108$; $P = 0.252$) rate of 0.38 days yr^{-1} for a total advance of approximately 5 days over the 14-yr study period.

These results are consistent with other satellite and regional observations of a long-term trend toward earlier growing seasons at high latitudes. Analyses of satellite vegetation indices have shown an approximate 8-day advance in the onset of the growing season at high latitudes from 1981 to 1991 (Myneni et al. 1997). A subsequent study using a longer satellite data record found that the onset of the growing season advanced by 8 days in North America and 6 days in Eurasia from 1982 to 1999 (Zhou et al. 2001). Other observations have shown an approximate 6-day advance in European spring bud-burst since the mid-1950s attributed to increases in spring air temperature (Menzel and Fabian 1999) and an advance of up to 7 days in the timing of atmospheric CO_2 draw down in spring and early summer from the 1960s to the early 1990s (Keeling et al. 1996). Visible-band satellite observations of weekly snow cover for the Northern Hemisphere have also shown a general advance in the timing of spring snow cover disappearance of 3–5 days $decade^{-1}$ since 1972 (Dye 2002).

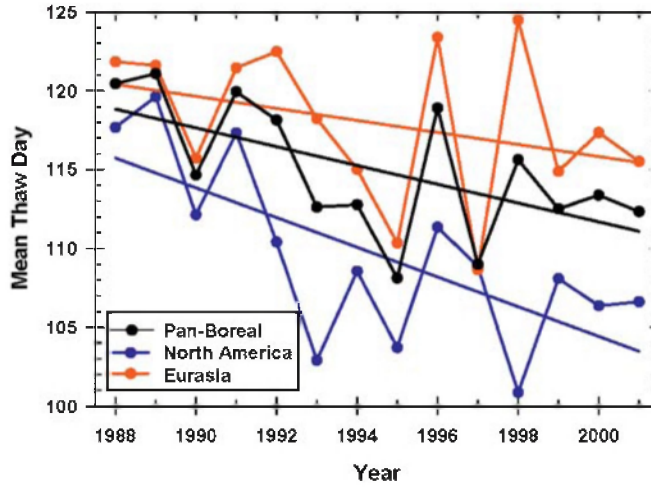

Figure 6. Trend of mean thaw day for the entire pan-boreal study region and for North America and Eurasia, separately. Mean primary thaw day for the pan-Arctic basin advanced approximately 8 days over the 14-yr SSM/I record. Regressions applied separately to North America and Eurasia thaw dates show the more pronounced thaw day advance in North America.

The apparent differences in SSM/I-based primary spring thaw trends between North America and Eurasia may reflect differences in regional precipitation and temperature patterns. A majority of the land area in North America shows an advancing rate in spring thaw (Figure 4). In Eurasia, however, the trends are mixed; while much of northern Siberia shows some advance in spring thaw, these trends are partially offset by delayed thaw trends over large portions of southern Eurasia. These results are generally consistent with observations from surface meteorological records over the last two decades, indicating that surface air temperatures are increasing in northern Eurasia but decreasing in southern Eurasia in response to enhanced storm activity in northern latitudes (). Analysis of tree-ring and climate data from the forest–tundra zone of Eurasia indicates that an increasing trend of winter precipitation has led to delayed snowmelt and growing season onset for sub-Arctic Eurasia (Vaganov et al. 1999). Similarly, satellite visible-band observations of regional snow cover from 1976 to 1990 show trends toward earlier spring snow cover disappearance in all regions except Eurasia (Foster et al. 1992). While the results of this investigation show a general advance in the primary spring thaw event across the pan-Arctic, they also show a high degree of spatial and interannual variability in thaw trends, with many areas experiencing near-neutral or delayed thaw trends of variable significance.

Figure 7 illustrates the correspondence of the thaw classification relative to point-scale temperature measurements in the soil and vegetation. The local maxima of the convolution CNF(t) correspond to major spring thaw events. For locations experiencing more than one thaw event, multiple local maxima are observed. The day of primary thaw t_p corresponds to the day of global maximum CNF(t_p). The data series from Zotino shows that t_p is observed during the seasonal soil warming trend. During 2001, a series of thaw events is detected prior to t_p, coinciding with episodic increases in daily mean air temperature occurring over about 40 days. As defined by the maximum in CNF(t), t_p occurs when the daily mean air temperature transitions above 0°C, while the soil active layer is thawing. Data from BNZ provide direct comparison with daily mean vegetation temperature. During 2000, t_p coincides with the onset of seasonal vegetation thaw. This represents the date liquid water is first available to the plant, providing a bound for the growing season onset. At the NOBS site, timing of primary snowmelt occurs many days prior to t_p during both 2000 and 2001. In these cases, although major thaw events are detected by CNF(t) during snowmelt, t_p occurs 20–30 days after these events with the arrival of more persistent warming. The data from these three sites illustrate that the classification scheme shows direct correlation to pronounced increases in the surface temperature field and associated landscape thaw, indicating that the SSM/I product for a 25-km grid compares favorably with the in situ point-scale data even when comparing a 25-km gridded remote sensing product to point-scale ground measurements. Past efforts in which the change detection approach has been applied to scatterometer measurements of near-daily temporal resolution have indicated that the primary source of thaw onset classification error is related to spatial heterogeneity of the surface freeze–thaw field (Kimball et al. 2004a). Potentially, spatial variability in the surface freeze–thaw state may limit the utility of the coarse-resolution SSM/I data in regions of high spatial complexity. Nevertheless, comparison of surface

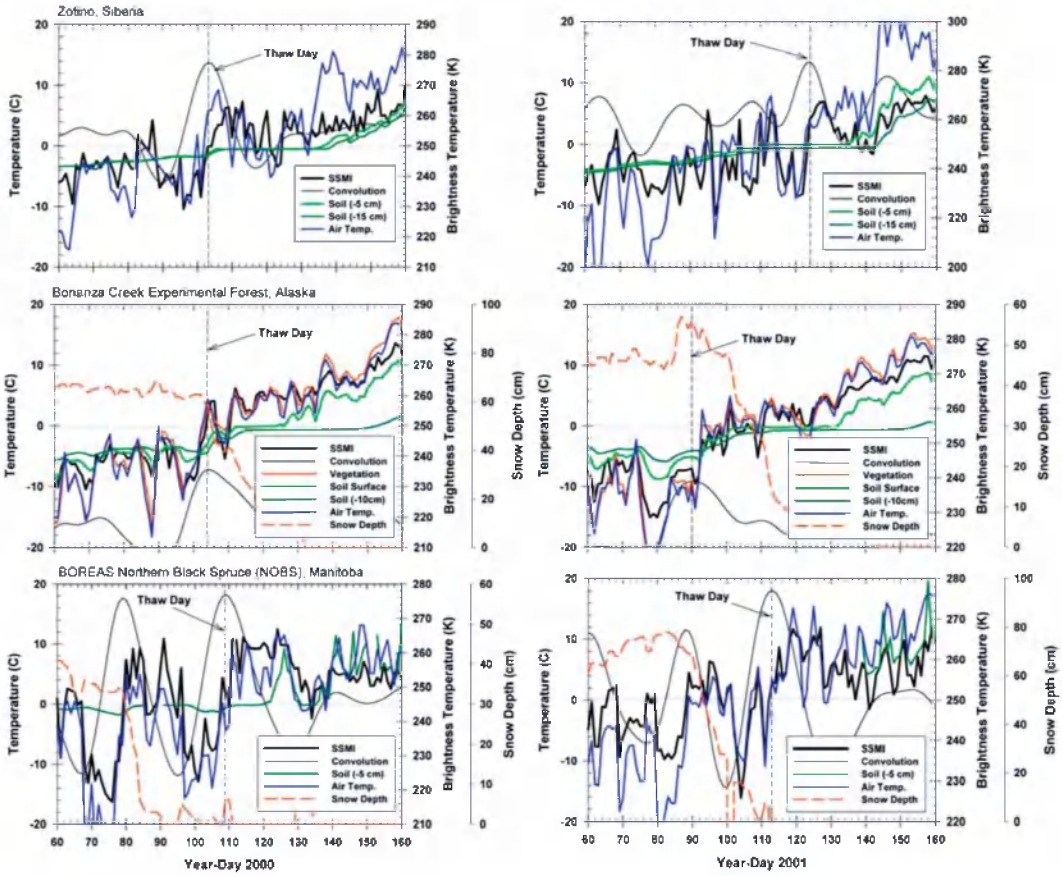

Figure 7. Comparison of SSM/I brightness temperature, thaw algorithm response (convolution), and ground measurements during springtime thaw of 2000 and 2001 for sites at (top) Zotino, in west-central Siberia; (middle) BNZ, in interior Alaska; and (bottom) the BOREAS NOBS Ameriflux tower site in northern Manitoba. At Zotino, T_B is compared with soil and air temperature; at BNZ, vegetation and air temperatures and snow depth measurements are included; NOBS shows comparison with soil and air temperatures and snow depth from a nearby weather station at the Thompson Airport at Manitoba. Air, soil, and vegetation temperatures are provided as daily mean values. The time of the maximum of the convolution integral, CNV(t), provides t_p, the thaw day. The local scale data, acquired at subregions within the 70 km $\times$ 45 km SSM/I footprint, illustrate the progression of snowmelt, and vegetation and soil thaw, as compared to the SSM/I-based thaw day.

temperature measurements to the algorithm performance as applied to SSM/I, as well as from past studies with spaceborne scatterometer data (Kimball et al. 2004b), demonstrates high correlation of classified freeze–thaw state to growing season onset.

The latitudinal distributions of boreal and tundra land-cover categories derived from a Moderate Resolution Imaging Spectroradiometer (MODIS) 1-km global land-

cover classification (Friedl et al. 2002) are shown in Figure 8 together with a plot of the mean thaw day by latitude for the 14-yr record. The time series of annual springtime thaw dates are compared to land cover to examine multiyear trends relative to land-cover distribution with latitude. Clear distinctions are seen in spatial patterns of seasonal thaw (i.e., latest thaw, earliest thaw, and mean thaw by latitude) and between boreal and Arctic landscapes. Timing of thaw spans more than 100 days across the region, beginning at lower latitudes and progressing at a rate of approximately 3 days deg^{-1} increase in latitude. Interannual variability in primary thaw day for tundra-dominated latitudes was on the order of 10–14 days, increasing to more than 20 days at lower latitudes. Although interannual variability in the mean thaw day for latitudes greater than 74°N and less than 48°N ranged as high as 30–60 days, this large variability is likely biased by the relatively small number of grid cells at the northern and southern extremes of the study region.

Segmentation of the study domain by general land-cover class allows examination of thaw patterns and trends within major biomes. Approximately 32% of the study region is composed of boreal evergreen coniferous and deciduous forests, while tundra occupies roughly 31% of the region based on a regional land-cover classification (Friedl et al. 2002). Table 2 lists the relative contribution and significance of these major biomes within the study domain to the advance in thaw date. Tundra shows a similar advancing trend in North America and Eurasia. The most pronounced advance is observed in evergreen needle leaf and mixed, deciduous evergreen forests of North America and leads to this region's dominance in thaw day advance shown in Figure 4.

Comparison of SSM/I-derived primary thaw and NOAA/CMDL seasonal CO_2 shape parameter anomalies showed strong evidence of a substantial link between

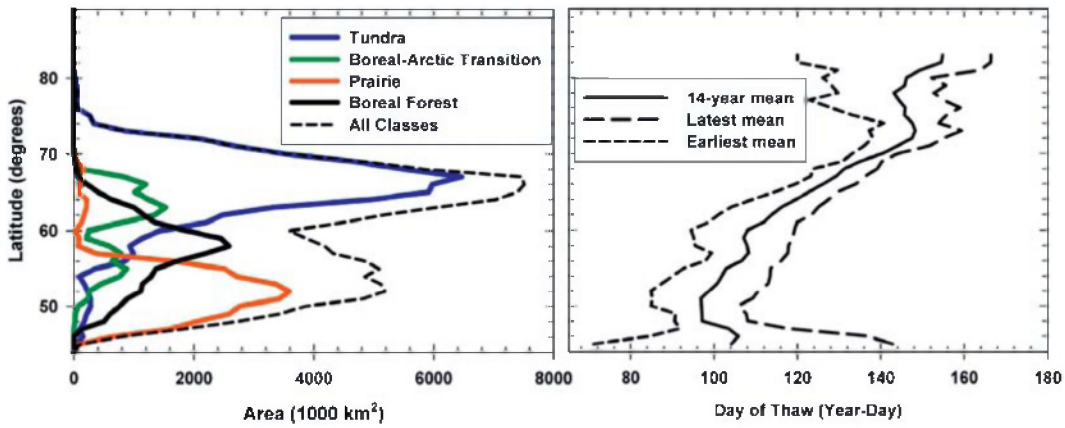

Figure 8. (left) The latitudinal distribution of boreal and tundra land-cover categories derived from the MODIS global land-cover classification is compared with (right) the latitudinal mean day of thaw for 1988–2001 and the maximum and minimum mean thaw days over the 14-yr series. Mean timing of thaw spans nearly 100 days across the region. Thaw is initiated at lower latitudes and progresses at a rate of approximately 2.5 days per degree increase in latitude. Variability in thaw timing ranges between 20 and 60 days.

Table 2. Advance in thaw day (days yr^{-1}) for 1988–2001 for the pan-boreal study domain and the North American and Eurasian subsets of that domain, segmented by land-cover class. Land-cover classes were defined using a MODIS 1-km resolution, global land-cover classification (Friedl et al. 2002).

	Pan-boreal region			North America			Eurasia		
Land cover	Advance	R^2	P value	Advance	R^2	P value	Advance	R^2	P value
Tundra	0.64	0.46	0.0076	0.64	0.31	0.037	0.63	0.33	0.032
Evergreen needle leaf	0.89	0.30	0.043	1.34	0.38	0.019	0.30	0.02	0.062
Deciduous needle leaf	0.49	0.06	0.38	N/A	N/A	N/A	0.49	0.06	0.38
Mixed forest	0.35	0.03	0.53	1.06	0.24	0.073	−0.01*	9.e-6	0.99

* The trend in Eurasian mixed forest is toward a later thaw date but is not significant.

spring thaw timing and seasonal atmospheric CO_2 cycles and associated vegetation productivity within the pan-Arctic study region. Statistically significant ($P < 0.1$) relationships between SSM/I-derived primary thaw and NOAA/CMDL–derived seasonal CO_2 shape parameter anomalies are presented in Table 3 and Figure 9. These results indicate that the timing of spring thaw is a major factor governing the pan-Arctic seasonal CO_2 cycle, particularly regarding impacts to regional photosynthetic activity (Figure 9). Spring thaw annual anomalies corresponded strongly to spring CO_2 zero crossing time anomalies ($r = 0.550$; $P = 0.042$). Thus, years with relatively early spring thaw events generally had earlier seasonal declines in atmospheric CO_2 and associated spring zero crossing times, while years with delayed thaw events had the opposite effect on spring CO_2 patterns. Spring thaw date anomalies were also directly proportional to annual minimum ($r = 0.633$; $P = 0.015$) and maximum ($r = 0.530$; $P = 0.051$) CO_2 anomalies. These results indicate a positive vegetation productivity response to earlier seasonal thawing for the northern high latitudes. In sub-Arctic and Arctic regions, much of the annual net photosynthetic uptake of atmospheric CO_2 is accumulated in early spring following seasonal snowmelt (Jarvis and Linder 2000; Running et al. 1999; Harazono et al. 2003). Abundant solar radiation, generally favorable air temperatures, and cool, moist soil conditions during this period promote photosynthetic uptake over respiration, resulting in rapid carbon sequestration and associated draw down of atmospheric CO_2 (Randerson et al. 1997). Potential vegetation productivity later in the growing season is limited by the rapid seasonal decline in day length and solar radiation, which is accelerated at increasingly

Table 3. Statistically significant ($P < 0.1$) relationships between SSM/I-derived primary thaw date anomalies (independent variable) and atmospheric CO_2 seasonal shape parameter anomalies (dependent variable) for the pan-Arctic study region.

Dependent variable	r value	P value	N
Spring CO_2 0-ppm crossing	0.550	0.042	14
CO_2 seasonal minimum	0.633	0.015	14
CO_2 seasonal maximum	0.530	0.051	14
Annual CO_2 uptake period*	0.536	0.059	13
Net photosynthesis*	0.705	0.007	13

* Previous year thaw date.

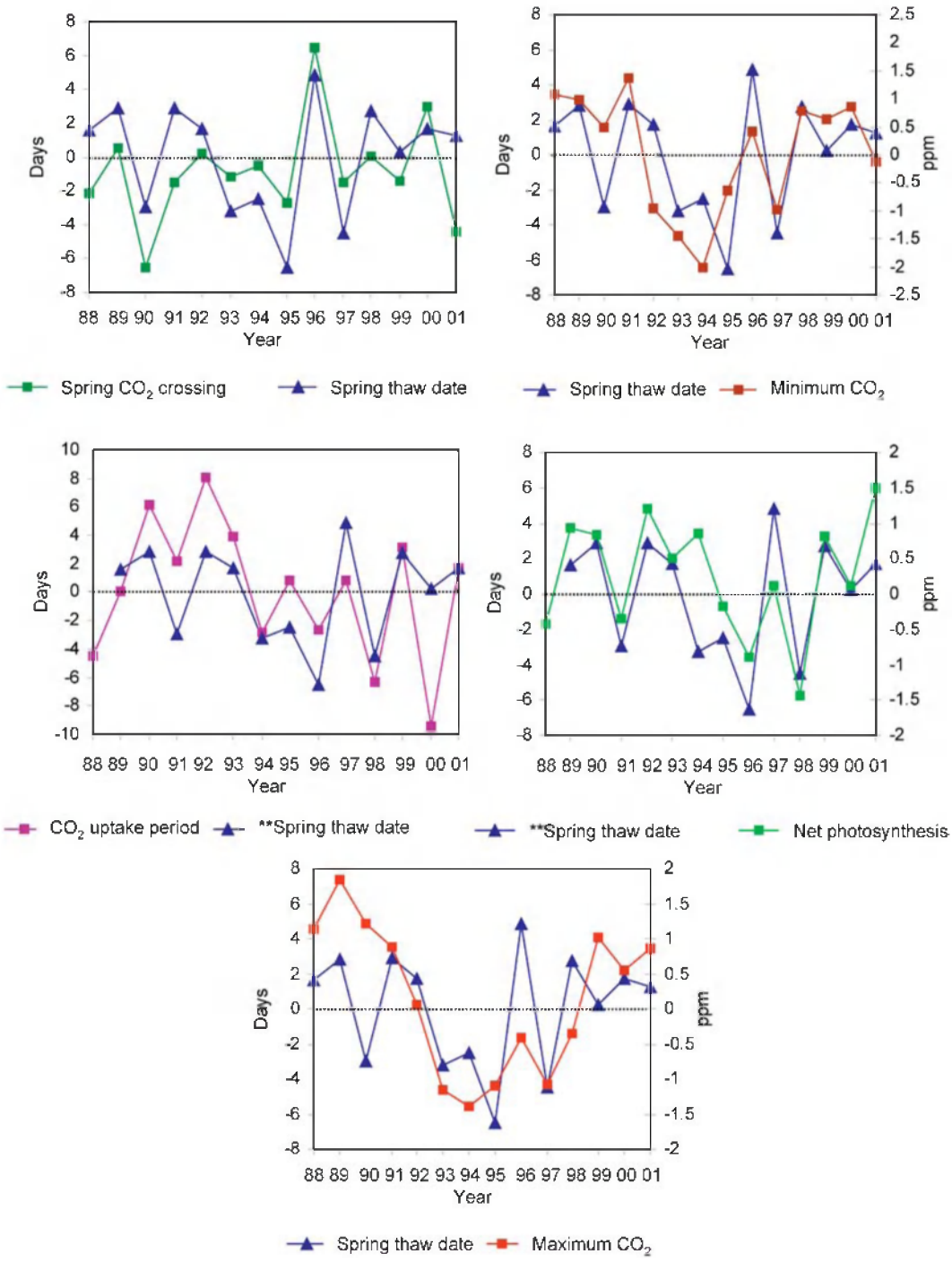

Figure 9. Plots of statistically significant ($P < 0.1$) relationships between NOAA/CMDL atmospheric CO_2 seasonal parameter anomalies and SSM/I-derived primary thaw event anomalies; negative anomalies denote earlier thawing and seasonal CO_2 draw down, greater CO_2 minima, lower maxima, shorter uptake period, and reduced net photosynthesis, while positive anomalies denote the opposite response relative to the long-term (1988–2001) record; the double asterisks ** represent the previous year thaw date.

higher latitudes (Kimball et al. 2004a). Warmer and drier soil conditions later in the season also promote increased respiration (Goulden et al. 1998). Thus, early spring thawing promotes an earlier and longer time interval of net photosynthetic carbon uptake and greater NPP, resulting in both earlier and larger seasonal decreases in atmospheric CO_2, while years with delayed spring thaw cycles promote the opposite response. The observed correspondence between annual maximum atmospheric CO_2 levels and spring thaw timing is likely an indirect effect of the relationship between spring thaw timing and vegetation productivity; years with earlier or later thawing events have generally lower or higher atmospheric CO_2 concentrations, respectively, overall due to vegetation carbon sequestration impacts on atmospheric CO_2.

The SSM/I-derived spring thaw date anomaly was directly proportional to subsequent-year annual terrestrial net photosynthesis ($r = 0.705$; $P = 0.007$) and growing-season-length ($r = 0.536$; $P = 0.059$) CO_2 anomalies. Thus, relatively early or late seasonal thaw events for a given year generally corresponded to respective reductions and enhancements in both net photosynthesis and growing season length for the subsequent year. This apparent delay in carbon cycle response to seasonal thaw may reflect an indirect respiration response to seasonal snowmelt and soil temperature. Both net photosynthesis and growing season length as defined in this investigation tend to be inversely proportional to respiration. Seasonal thaw and associated spring snowpack depletion generally coincide with a rapid reduction in surface albedo and a corresponding increase in net radiation at high latitudes, particularly for nonforested tundra (Zhang et al. 2003). Thus, earlier snowmelt promotes increased seasonal solar energy loading into soils, which may promote warmer soil temperatures, development of deeper soil active-layer depths, and increased early season respiration rates the following year. Earlier snowmelt also appears to promote vegetation productivity, which may enhance subsequent-year respiration rates further through increased biomass and litter production and decomposition (Kimball et al. 2004a).

Vegetation productivity at high latitudes is generally limited by soil nutrient availability, especially nitrogen, N (Shaver and Jonasson 2001; Schimel et al. 1996). Net primary production in these regions is largely sustained by internal N recycling through decomposition of litter and soil organic matter late in the growing season, after most of the current year's growth has occurred. This can result in a temporal lag between annual NPP and seasonal weather patterns for a given year (Shaver and Jonasson 2001). In tundra and boreal soils, much of the annual nutrient flux of plant-available N is rapidly released during seasonal snowmelt and soil thaw. Years with relatively early seasonal thawing have generally greater productivity, which may immobilize critical nutrients in vegetation and microbial biomass, resulting in reduced productivity the following year. Alternatively, years with delayed seasonal thawing and reduced plant productivity may promote increased nutrient availability and associated plant productivity the following year. These phenomena have been observed at the scale of individual communities but require further study at regional and continental scales.

No significant relationships were found between spring thaw anomalies and annual CO_2 uptake period, CO_2 semiannual photosynthesis (P), respiration (R), or

P:R ratio anomalies for a given year. These results likely reflect additional impacts to the seasonal atmospheric CO_2 cycle such as temperature, cloud cover, and precipitation patterns, which are highly variable and strongly affect both photosynthesis and respiration processes at high latitudes. While early spring thaws may enhance photosynthesis in spring, cloudy or dry conditions and relatively warm temperatures may promote respiration release over photosynthetic uptake of CO_2 later in the season. The timing of freezing temperatures and arrival of seasonal snow cover in the fall also influence growing season length and soil respiration. Fires and other regional disturbance impacts such as the 1991 Mt. Pinatubo volcanic eruption are known to affect high-latitude CO_2 uptake and respiration processes and are likely additional factors influencing the shape of the seasonal CO_2 cycle independent of spring thaw timing (Lucht et al. 2002; Zimov et al. 1999).

4. Conclusions

The results of this study identify strong linkages between the timing of spring thaw, growing season initiation, and the timing and relative magnitude of seasonal uptake of atmospheric CO_2 by terrestrial net photosynthesis at high northern latitudes. Years with relatively early seasonal thawing appear to promote both earlier and greater seasonal uptake of atmospheric CO_2 through enhanced NPP and associated carbon sequestration by terrestrial vegetation, while years with delayed seasonal thawing promote the opposite response. Our results also indicate that the pan-Arctic region exhibited a trend toward earlier seasonal thawing and growing season onset from 1988 to 2001. Other studies for the region have shown evidence of earlier seasonal draw down and increased seasonal amplitude of atmospheric CO_2, earlier onset of vegetation greening, and increased NPP over the same period as this investigation. Additionally, significant relationships have been observed between spring thaw timing and annual NPP and net CO_2 exchange in boreal forests. These results imply that the timing of seasonal thawing in spring has a major impact on terrestrial NPP and net carbon exchange at high latitudes. As boreal and subalpine evergreen coniferous forests sequester significantly more of their annual NPP on a daily basis in the spring relative to the fall (Kimball et al. 2004b), timing of growing season initiation has a greater impact relative to annual NPP than timing of growing season termination. The initiation of the growing season occurred earlier, on average, over the time period addressed in this study and may be a major mechanism driving observed atmospheric CO_2 seasonal cycle advances, vegetation greening, and enhanced productivity for the northern high latitudes.

Previous investigations of long-term trends in the visible near-infrared satellite record have shown evidence of recent advances in the onset of vegetation greening and the growing season at high latitudes (e.g., Myneni et al. 1997). However, the validity of these trends have been questioned because of the coarse 10–15-day temporal compositing of the data required to mitigate atmospheric aerosol effects, problems with sensor and navigational drift, intercalibration of successive instruments, data contamination from volcanic eruptions, and bidirectional effects (e.g., Gutman and Ignatov 1995; Gutman 1999; Cihlar et al. 1998). Existing

surface biophysical monitoring networks provide detailed information on long-term trends with relatively high accuracy but generally over limited spatial extents, especially at high latitudes. The microwave-based information from SSM/I and other active and passive satellite microwave sensors are sensitive to landscape freeze–thaw state transitions associated with the onset of the growing season at high latitudes. The relative independence of these data from atmospheric aerosol contamination and solar illumination provide the potential for spatially explicit, daily monitoring of this important biophysical variable at high latitudes where global change is projected to occur first and may already be occurring, with the greatest magnitude and with significant feedbacks to global climate and the carbon cycle. While current satellite microwave sensors have the potential to resolve pan-Arctic growing season trends with better temporal (i.e., daily) accuracy than other existing satellite and surface biophysical monitoring networks, their ability to accurately resolve these trends at finer (<25 km) spatial scales is less certain, particularly for topographically complex landscapes. However, new satellite platforms are currently under development that will allow improved spectral and spatial characterization of this important biophysical variable (ENT).

Acknowledgments. The authors gratefully acknowledge Dr. Martin Heimann (Max-Planck-Institute for Biogeochemisty, Jena, Germany) and Dr. Olga Shibistova (Sukachev Forest Institute, Russian Academy of Sciences, Krasnojarsk, Russia) for providing the Zotino dataset. NOAA/NASA Pathfinder SSM/I Level 3 EASE-Grid Brightness Temperatures were obtained from the EOSDIS NSIDC Distributed Active Archive Center (NSIDC DAAC), University of Colorado. We are grateful for the assistance with data processing and algorithm development provided by Charles Thompson, Mauricio Cordero, Daniel Wu, Veasna Sok, and Jason Kwok-San Lee. This work was funded by grants from the National Science Foundation's Office of Polar Programs and the National Aeronautics and Space Administration Office of Earth Science Enterprise. This work was carried out at the Jet Propulsion Laboratory, California Institute of Technology, and at the University of Montana, Missoula, under contract to the National Aeronautics and Space Administration.

References

Armstrong, R. L., and M. J. Brodzik, 1995: An earth-gridded SSM/I data set for cryospheric studies and global change monitoring. *Adv. Space Res.,* **16** (10), 155–163.

Armstrong, R. L., K. W. Knowles, M. J. Brodzik, and M. A. Hardman, 1994: DMSP SSM/I Pathfinder daily EASE-Grid brightness temperatures (1994–2002). National Snow and Ice Data Center, Boulder, CO, digital media and CD-ROM.

Baldocchi, D., R. Valentini, S. Running, W. Oechel, and R. Dahlman, 1996: Strategies for measuring and modelling carbon dioxide and water vapour fluxes over terrestrial ecosystems. *Global Change Biol.,* **2,** 159–168.

Betts, A. K., P. Viterbo, A. Beljaars, H.-L. Pan, S.-Y. Hong, M. Goulden, and S. Wofsy, 1998: Evaluation of land-surface interaction in ECMWF and NCEP/NCAR reanalysis models over grassland (FIFE) and boreal forest (BOREAS). *J. Geophys. Res.,* **103** (D18), 23 079–23 085.

Black, T. A., and Coauthors, 2000: Increased carbon sequestration by a boreal deciduous forest in years with a warm spring. *Geophys. Res. Lett.,* **27,** 1271–1274.

Canny, J. F., 1986: A computational approach to edge detection. *IEEE Trans. Pattern Anal. Mach. Intell.,* **8,** 679–698.

Ciais, P., P. P. Tans, M. Trolier, J. W. C. White, and R. J. Francey, 1995: A large Northern Hemisphere terrestrial CO_2 sink indicated by the 13C/12C ratio of atmospheric CO_2. *Science,* **269,** 1098–1101.

Cihlar, J., J. M. Chen, Z. Li, F. Huang, R. Latifovic, and R. Dixon, 1998: Can interannual land surface signal be discerned in composite AVHRR data? *J. Geophys. Res.,* **103** (D18), 23 163–23 172.

Clark, M. P., M. C. Serreze, and D. A. Robinson, 1999: Atmospheric controls on Eurasian snow extent. *Int. J. Climatol,* **19,** 27–40.

Conway, T. J., P. P. Tans, L. S. Waterman, K. W. Thoning, D. R. Kitzis, K. A. Masarie, and N. Zhang, 1994: Evidence for interannual variability of the carbon cycle from the NOAAA/CMDL global air sampling network. *J. Geophys. Res.,* **99,** 22831–22855.

Dye, D. G., 2002: Variability and trends in the annual snow-cover cycle in Northern Hemisphere land areas, 1972–2000. *Hydrol. Processes,* **16,** 3065–3077.

Entekhabi, D., and Coauthors, 2004: The Hydrosphere state (Hydros) satellite mission: An earth system pathfinder for global mapping of soil moisture and land freeze/thaw. *IEEE Trans. Geosci. Remote Sens.,* **42,** 2184–2195.

Erickson, D. J., and Coauthors, 1996: The seasonal cycle of atmospheric CO_2: A study based on the NCAR Community Climate Model (CCM2). *J. Geophys. Res.,* **101,** 15 079–15 097.

Fan, S., M. Gloor, J. Mahlman, S. Pacala, J. Sarmiento, T. Takahashi, and P. Tans, 1998: A large terrestrial carbon sink in North America implied by atmospheric and oceanic carbon dioxide data and models. *Science,* **282,** 442–446.

Foster, J. L., J. W. Winchester, and E. G. Dutton, 1992: The date of snow disappearance on the Arctic tundra as determined from satellite, meteorological station and radiometric in situ observations. *IEEE Trans. Geosci. Remote Sens.,* **30,** 793–798.

Friedl, M. A., and Coauthors, 2002: Global land cover from MODIS: Algorithms and early results. *Remote Sens. Environ.,* **83,** 135–148.

Frolking, S., and Coauthors, 1996: Modeling temporal variability in the carbon balance of a spruce/moss boreal forest. *Global Change Biol.,* **2,** 343–366.

Frolking, S., K. C. McDonald, J. Kimball, J. B. Way, R. Zimmermann, and S. W. Running, 1999: Using the space-borne NASA scatterometer (NSCAT) to determine the frozen and thawed seasons of a boreal landscape. *J. Geophys. Res.,* **104** (D22), 27 895–27 907.

Goulden, M. L., and Coauthors, 1998: Sensitivity of boreal forest carbon balance to warming. *Science,* **279,** 214–217.

Gutman, G. G., 1999: On the monitoring of land surface temperatures with the NOAA/AVHRR: Removing the effect of satellite orbit drift. *Int. J. Remote Sens.,* **20,** 3407–3413.

Gutman, G., and A. Ignatov, 1995: Global land monitoring from AVHRR—Potential and limitations. *Int. J. Remote Sens.,* **16,** 2301–2309.

Hall, C. A. S., C. A. Ekdahl, and D. E. Wartenberg, 1975: A fifteen-year record of biotic metabolism in the Northern Hemisphere. *Nature,* **255,** 136–138.

Hanqin, T., C. A. S. Hall, and Y. Qi, 2000: Increased biotic metabolism of the biosphere inferred from observed data and models. *Sci. China,* **43** (1), 58–68.

Harazono, Y., M. Mano, A. Miyata, R. C. Zulueta, and W. C. Oechel, 2003: Inter-annual carbon dioxide uptake of a wet sedge tundra ecosystem in the Arctic. *Tellus,* **55B,** 215–231.

Heimann, M., and Coauthors, 1998: Evaluation of terrestrial subcarbon cycle models through

simulations of the seasonal cycle of atmospheric CO_2: First results of a model intercomparison study. *Global Biogeochem. Cycles,* **12,** 1–24.

Houghton, J. T., L. G. Meira Filho, B. A. Callander, N. Harris, A. Kattenberg, and K. Maskell, 1996: *Climate Change 1995: The Science of Climate Change*. Cambridge University Press, 584 pp.

Jacoby, G. C., R. D. d'Arrigo, and T. Davaajamts, 1996: Mongolian tree rings and 20th-century warming. *Science,* **273,** 771–773.

Jarvis, P., and S. Linder, 2000: Constraints to growth of boreal forests. *Nature,* **405,** 904–905.

Karl, T. R., F. Bretherton, W. Easterling, C. Miller, and K. Trenberth, 1995: Long-term climate monitoring by the global climate observing system (GCOS). *Climatic Change,* **31** (2–4), 135–147.

Keeling, C. D., J. F. S. Chin, and T. P. Whorf, 1996: Increased activity of northern vegetation inferred from atmospheric CO_2 measurements. *Nature,* **382,** 146–149.

Keyser, A. R., J. S. Kimball, R. R. Nemani, and S. W. Running, 2000: Simulating the effects of climate change on the carbon balance of North American high latitude forests. *Global Change Biol.,* **6,** 185–195.

Kimball, J., K. C. McDonald, A. R. Keyser, S. Frolking, and S. W. Running, 2001: Application of the NASA Scatterometer (NSCAT) for classifying the daily frozen and non-frozen landscape of Alaska. *Remote Sens. Environ.,* **75,** 113–126.

Kimball, J., K. C. McDonald, S. Frolking, and S. W. Running, 2004a: Radar remote sensing of the spring thaw transition across a boreal landscape. *Remote Sens. Environ.,* **89,** 163–175.

Kimball, J., K. C. McDonald, S. W. Running, and S. Frolking, 2004b: Satellite radar remote sensing of seasonal growing seasons for boreal and sub-alpine evergreen forests. *Remote Sens. Environ.,* **90,** 243–258.

Lucht, W., and Coauthors, 2002: Climatic control of the high-latitude vegetation greening trend and Pinatubo effect. *Science,* **296,** 1687–1689.

McGuire, A. D., and Coauthors, 2004: Land cover and land use change in Alaska and Canada. *Land Change Science: Observing, Monitoring, and Understanding Trajectories of Change on the Earth's Surface,* G. Gutman et al., Eds., *Remote Sensing and Digital Image Processing,* Vol. 6, 461 pp.

Menzel, A., and P. Fabian, 1999: Growing season extended in Europe. *Nature,* **397,** 659–661.

Myneni, R. B., C. D. Keeling, C. J. Tucker, G. Asrar, and R. R. Nemani, 1997: Increased plant growth in the northern high latitudes from 1981–1991. *Nature,* **386,** 698–702.

Nemani, R. R., C. D. Keeling, H. Hashimoto, W. M. Jolly, S. C. Piper, C. J. Tucker, R. B. Myneni, and S. W. Running, 2003: Climate-driven increases in global terrestrial net primary production from 1982 to 1999. *Science,* **300,** 1560–1563.

Pielke, R. A., and P. L. Vidale, 1995: The boreal forest and the polar front. *J. Geophys. Res.,* **100,** 25755–25758.

Randerson, J. T., M. V. Thompson, T. J. Conway, I. Y. Fung, and C. B. Field, 1997: The contribution of terrestrial sources and sinks to trends in the seasonal cycle of atmospheric carbon dioxide. *Global Biogeochem. Cycles,* **11,** 535–560.

Randerson, J. T., C. B. Field, I. Y. Fung, and P. P. Tans, 1999: Increases in early season ecosystem uptake explain recent changes in the seasonal cycle of atmospheric CO_2 at high northern latitudes. *Geophys. Res. Lett.,* **26,** 2765–2768.

Rawlins, M. A., K. C. McDonald, S. Frolking, R. B. Lammers, M. Fahnestock, J. S. Kimball, and C. J. Vörösmarty, 2005: Remote sensing of pan-Arctic snowpack thaw using the SeaWinds Scatterometer. *J. Hydrol.,* in press.

Robinson, D. A., K. F. Dewey, and R. R. Heim, 1993: Global snow cover monitoring: An update. *Bull. Amer. Meteor. Soc.,* **74,** 1689–1696.

Running, S., J. B. Way, K. C. McDonald, J. Kimball, and S. Frolking, 1999: Radar remote sensing proposed for monitoring freeze–thaw transitions in boreal regions. *Amer. Geophys. Union Newsl.,* **80** (19), 220–221.

Schimel, J. P., K. Kielland, and F. S. Chapin III, 1996: Nutrient availability and uptake by tundra plants. *Landscape Function and Disturbance in Arctic Tundra,* J. F. Reynolds and J. D. Tenhunen, Eds., Vol. 120, Springer-Verlag, 203–221.

Serreze, M. C., and Coauthors, 2000: Observational evidence of recent change in the northern high-latitude environment. *Climatic Change,* **46** (1–2), 159–207.

Shaver, G., and S. Jonasson, 2001: Productivity of arctic ecosystems. *Terrestrial Global Productivity*, J. Roy, B. Saugier, and H. A. Mooney, Eds., Academic Press, 189–210.

Tanja, S., and Coauthors, 2003: Air temperature triggers the recovery of evergreen boreal forest photosynthesis in spring. *Global Change Biol.,* **9,** 1410–1426.

Tans, P. P., I. Y. Fung, and T. Takahashi, 1990: Observational constraints on the global CO_2 budget. *Science,* **247,** 1431–1438.

Ulaby, F. T., R. K. Moore, and A. K. Fung, 1986: *Microwave Remote Sensing: Active and Passive*, Vol. 1, Artec House, 456 pp.

Vaganov, E. A., M. K. Hughes, A. V. Kirdyanov, F. H. Schweingruber, and P. P. Silkin, 1999: Influence of snowfall and melt timing on tree growth in subarctic Eurasia. *Nature,* **400,** 149–151.

Watson, R. T., M. C. Zinyowera, R. H. Moss, and D. J. Dokken, Eds., 1998: *The Regional Impacts of Climate Change: An Assessment of Vulnerability*. Cambridge University Press, 517 pp.

Wirth, C., and Coauthors, 1999: Above-ground biomass and structure of pristine Siberian Scots pine forests as controlled by competition and fire. *Oecologia,* **121,** 66–80.

Wismann, V., 2000: Monitoring of seasonal thawing in Siberia with ERS scatterometer data. *IEEE Trans. Geosci. Remote Sens.,* **38,** 1804–1809.

Zhang, T., and R. L. Armstrong, 2001: Soil freeze/thaw cycles over snow-free land detected by passive microwave remote sensing. *Geophys. Res. Lett.,* **28,** 763–766.

Zhang, T., T. Scambos, T. Haran, L. D. Hinzman, R. G. Barry, and D. L. Kane, 2003: Ground-based and satellite-derived measurements of surface albedo on the North Slope of Alaska. *J. Hydrometeor.,* **4,** 77–91.

Zhou, L., C. J. Tucker, R. K. Kaufmann, D. Slayback, N. V. Shabanov, and R. B. Myneni, 2001: Variations in northern vegetation activity inferred from satellite data of vegetation index during 1981 to 1999. *J. Geophys. Res.,* **106** (D17), 20 069–20 083.

Zimmermann, R., E.-D. Schulze, C. Wirth, E. Schulze, K. C. McDonald, N. N. Vygodskaya, and W. Ziegler, 2000: Canopy transpiration in a chronosequence of central Siberian pine forests. *Global Change Biol.,* **6,** 25–37.

Zimov, S. A., S. P. Davidov, G. M. Zimova, A. I. Davidova, F. S. Chapin III, M. C. Chapin, and J. F. Reynolds, 1999: Contribution of disturbance to increasing seasonal amplitude of atmospheric CO_2. *Science,* **284,** 1973–1976.